



Parkinson's disease detection and stage classification: quantitative gait evaluation through variational mode decomposition and DCNN architecture

Balaji E, Vinodh Kumar Elumalai, Dhanasekaran Sandhiya, R. M. Swarna Priya & S. P. Shanthalrajah

To cite this article: Balaji E, Vinodh Kumar Elumalai, Dhanasekaran Sandhiya, R. M. Swarna Priya & S. P. Shanthalrajah (2024) Parkinson's disease detection and stage classification: quantitative gait evaluation through variational mode decomposition and DCNN architecture, Connection Science, 36:1, 2383894, DOI: [10.1080/09540091.2024.2383894](https://doi.org/10.1080/09540091.2024.2383894)

To link to this article: <https://doi.org/10.1080/09540091.2024.2383894>



© 2024 The Author(s). Published by Informa UK Limited, trading as Taylor & Francis Group.



Published online: 09 Aug 2024.



Submit your article to this journal



Article views: 545



View related articles



CrossMark

View Crossmark data

Parkinson's disease detection and stage classification: quantitative gait evaluation through variational mode decomposition and DCNN architecture

Balaji E^a, Vinodh Kumar Elumalai^b, Dhanasekaran Sandhiya^c, R. M. Swarna Priya^d and S. P. Shanthalarajah^d

^aSchool of Computer Science Engineering and Information Systems, Vellore Institute of Technology, Vellore, India; ^bSchool of Electrical Engineering, Vellore Institute of Technology, Vellore, India; ^cDepartment of Statistics and Data Science, National University of Singapore, Singapore; ^dSchool of Information Technology & Engineering, Vellore Institute of Technology, Vellore, India

ABSTRACT

Parkinson's disease (PD) is a progressive, debilitating neurological movement disorder that affects the person's muscle control, movement, speech, cognition and dexterity. For diagnosing PD in a clinical setting, in addition to the neurological examinations, clinicians use the unified Parkinson disease rating scale (UPDRS) to assess the motor and non-motor impairments. Such a clinical assessment highly depends on the experience and expertise of the clinicians, and it may result in biased evaluation. Hence, to assist the clinicians, we put forward a gait analysis-based deep convolutional neural network (DCNN) framework which leverages the potentials of variational mode decomposition (VMD) technique with the recurrence plots (RP) to enhance the PD severity classification performance. Specifically, transforming the VMD modes of vertical ground reaction force (VGRF) time series data into two-dimensional texture images to capture the temporal dependency, this work trains the DCNN classifier through recurrence images for its ability to extract the discriminative features among the PD severity levels. For evaluation, this study utilises the VGRF dataset of 93 PD subjects and 73 healthy controls from Physiobank for three different walking tests. Consequently, utilising VMD, RP and DCNN in a unified framework, this investigation shows that the PD severity rating can be significantly enhanced through DCNN model that is trained using RP of dominant intrinsic mode functions (IMFs). The novelty of the proposed framework lies in identifying the prominent gait biomarkers through dominant IMFs from power spectral analysis for reducing the computational burden of DCNN. Moreover, to handle the data over-fitting issue in the classifier, L2 regularisation technique, which penalises the weight parameters of the nodes, is used in combination with the dropout

ARTICLE HISTORY

Received 13 August 2023

Accepted 18 July 2024

KEYWORDS

Parkinson's disease; gait analysis; variational mode decomposition; recurrence plot; deep convolutional neural network

layer. Experimental results underscore that the proposed VMD-RP-DCNN architecture can address the spectral overlapping issue in VGRF decomposition and achieve an average PD severity prediction accuracy of 98.45%.

1. Introduction

Parkinson disease is a chronic neurological disorder, which predominantly affects the muscle movement, balance, and coordination. PD, which manifests a multitude of motor and non-motor symptoms, is caused majorly because of lack of a chemical messenger in the substantia nigra called dopamine (Skaramagkas et al., 2023). Few of the primary motor manifestations of PD are: rest tremor, bradykinesia, impaired posture, and rigidity. Likewise, the typical non-motor deficits are: fatigue, orthostatic hypertension, depression, and sleep disorder. Even though currently, PD is incurable, the early diagnosis is essential to slow down the progression so that the person can lead a quality life. For diagnosing PD, investigating the biosignals such as handwriting, tremor, gait and speech assists in accurately evaluating the motor symptoms of patients, thereby offering objective and additional information to clinicians to make precise and timely interventions of appropriate medication (Alharthi et al., 2019).

From diagnostic viewpoint, gait analysis is an important approach because the PD patients manifest the gait abnormalities as one of the earliest symptoms (Alharthi & Ozanyan, 2019). Hence, the gait assessment can be used for identifying the early onset of PD. The Parkinsonian gait is primarily characterised by a large stride to stride variability, a slow gait cycle, a long stance phase and a toe-off. To identify the presence of PD, generally, the clinicians assess the walking pattern by visual inspection along with the UPDRS. Notwithstanding, the gait evaluation is highly subjective because it majorly rests on the expertise of the neurologists and there is no effective tool available to predict the presence of PD (Alharthi & Ozanyan, 2019). Moreover, the progression of PD varies according to the age, health condition and other intrinsic factors. Therefore, in order to alleviate the misdiagnosis problems due to manual assessment, automated systems are being designed to classify the PD from gait cycle (Schwab & Karlen, 2019). Even though gait analysis-based PD diagnosis has attracted considerable attention, for quantitative assessment of PD and its stages, a finer investigation on the hidden gait biomarkers is needed for realising an effective classifier tool (Zhou et al., 2019). In literature, considerable research attention has been paid to explore the potential of the machine learning (ML) based classifiers to diagnose PD based on gait evaluation (ul Haq et al., 2022). For instance, Abdulhay et al. (2018) studied the efficacy of SVM classifier to diagnose the PD through kinematic parameters and achieved a mean accuracy of 92.7%. Balaji et al. (2020) studied the performance of four ML classifiers such as DT,SVM,KNN and BC for PD severity rating based on spatiotemporal analysis of gait. Joshi et al. (2017) analysed the wavelet features from gait data and utilised SVM to distinguish between the healthy and PD subjects. Likewise, some of the prominent gait-based PD prediction approaches reported in the literature are deterministic learning (Zeng et al., 2016), recurrence quantification analysis (Prabhu et al., 2020), and extreme learning machine (Oung et al., 2018). For detailed review on ML-based PD diagnosis, the readers can refer to Figueiredo et al. (2018). In spite of the remarkable performance

of aforementioned ML algorithms for PD diagnosis, their major limitation is the demand for manual feature extraction, which may not be computationally intensive. Therefore, to avoid the manual feature engineering, in this work, we explore the efficacy of DCNN classifier models for multi-class PD severity rating. The VGRF gait dataset obtained using foot worn sensors from Physionet is used for assessing the efficacy of the proposed approach (PD: P.D.D., 2020). The primary motivation for the proposed VGRF decomposition based DCNN framework is as follows. Even though CNN can extract gait biomarkers, the major limitation is that through convolution the raw VGRF signal is only downsampled, leaving the essential characteristics of gait pattern not being completely retrieved. Hence, for effective feature extraction, the decomposition techniques can be used in combination with CNN. In this regard, we utilise the VMD technique, which is an efficient and adaptive non-recursive decomposition technique highly suitable for nonlinear and non-stationary signals such as VGRF. Firstly, the VGRF signals of the healthy and PD subjects are decomposed into several narrow-band intrinsic modes and the dominant modes in the decomposed VGRF signals are identified through spectral analysis. Then, the dominant IMFs are transformed into two-dimensional textural images through RPs for capturing periodical nature in the time series data of healthy and PD subjects and training the DCNN with RPs for enhanced PD stage prediction performance. Specifically, modelling gait-based PD severity prediction problem as an RP-based DCNN image classification task, we utilise the VMD and spectral analysis approach for representing the dominant IMFs as recurrence images to improve the possibility of extracting invisible features of the 1D signals. Moreover, we compare the performance of the proposed approach with that of the vanilla DCNN (VDCNN) trained using the VGRF time series signal to highlight the improvement in PD stage classification performance. In this clinical context, the notable contributions of our study are as follows.

- To handle nonlinear and non-stationary dynamics of gait signals, we adopt a VMD technique and perform the spectral analysis to identify the prominent gait biomarkers through dominant IMFs.
- To enhance PD severity prediction performance of DCNN classifier model, we propose to utilise the visual features of VGRF time series data through recurrence plots (RP) and demonstrate the potential based on the gait signals from three walking tests.
- Utilising the Adam optimiser for solving the loss function, we achieve an average classification accuracy of 98.45% for PD severity rating based on H & Y scale.

The rest of the article is formulated as follows. Section 2 presents the review of related results reported in the literature on PD diagnosis using gait analysis. Section 3 presents the dataset considered for the proposed study. Section 4 details the proposed methodology and describes the performance metrics considered for assessing the efficacy of the DCNN classifier. Section 5 discusses the results of VDCNN and the proposed DCNN framework through confusion matrix. Finally, the concluding remarks of the article is presented in Section 6.

2. Related work

This section critically evaluates noteworthy investigations on PD diagnosis based on gait signal analysis. Several methods to quantitatively assess the gait variability for PD diagnosis

have been reported. Particularly, the gait assessment using the time-frequency domain, spatio-temporal domain using ML- and DL algorithms are discussed.

Kim et al. (2018) proposed a CNN structure for quantifying the severity of PD patients based on UPDRS scale. Using the custom designed wearable device fitted with a gyroscope and a tri-axial accelerometer, they collected tremor signals from 92 patients and transformed the gyroscope and accelerometer signals into a 2D image for CNN input. Through tuning of hyper-parameters of CNN that could discriminate the level of tremor severity, authors achieved an average accuracy of 85%. However, the repeatability of the CNN model to quantify the tremor needs to be assessed when the change happens in patients state and environmental conditions.

To analyse the nervous system and model the transitions in PD patients during start and stop movements, Vásquez-Correa et al. (2018) put forward a deep learning architectures based multimodal assessment technique, fusing the information from three modalities: speech, handwriting and gait. The specific motor dysfunctions in upper/lower limbs along with the impairments in speech were examined to predict the PD stages based on MDS-UPDRS scale. Based on the interpretation of the feature map obtained from CNN, they not only showed that the classification accuracy could be improved but also evaluated the robustness of their approach through the speech impairment analysis in three different languages. It was reported that even though the gait and speech analysis could provide better results compared to handwriting assessment, to address the influence of the language further experiments on sentences, texts and spontaneous speech signals could be performed.

For diagnosing the presence of PD, Abdulhay et al. (2018) utilised a gait and tremor signals from Physionet and presented a pulse duration and peak detection measuring techniques to extract the spatiotemporal features. To pre-process the raw VGRF dataset, they employed a type II Chebyshev high pass filter and obtained the spatiotemporal features including stride time, swing time, heel strike and toe off in order to build a feature set based on foot strike profile variability. Transforming the time series data into frequency domain through FFT for distinguishing the amplitude variation, they used PSD of tremor signals to differentiate between tremor at rest and other tremors. Medium tree and medium Gaussian SVM were employed to categorise the healthy subjects and PD patients. However, this approach was limited to binary classification wherein only the presence of PD was diagnosed and the stages were not identified.

Pereira et al. (2018) put forward a hand written dynamics assessment technique for PD identification. Using the smart pen that captures the finger-grip, axial pressure, tilt angle in X, Y and Z directions, they conducted few handwritten exams such as drawing circles and spirals on a paper. To acquire prominent features from every handwritten exam and improve the classification accuracy, ensemble of CNNs was used. By mapping the signals acquired from smartpen for the different images drawn by PD patients and healthy controls, they compared the performance of ML algorithms with those of the two distinct CNN architectures. Even though better classification accuracy was obtained using CNN architecture compared to machine learning approaches, the paper does not report any approach for minimising the feature space dimension.

For early stage monitoring of PD, Perumal and Sankar (2016) explored the effect of using both tremor and gait features obtained from the wearable sensors. Extracting the kinetic and spatiotemporal features from gait cycle, they employed a LDA classifier to distinguish

between control subjects and PD patients. In tremor analysis, to improve the frequency resolution and minimise the spectral leakage, a Haan window was utilised. Testing the performance of the approach using the dataset from Physionet, they achieved an average classification accuracy of 86.9%. Nevertheless, this method was limited to only two-class classification problem and failed to assess the stages of PD. Vidya and Sasikumar (2021) presented a multi-class SVM technique to predict the severity of PD based on the gait variability analysis. Extracting the spatio and temporal features from the gait cycles, they have trained the SVM model with optimal feature set identified using the correlation technique. In a similar direction, Khera and Kumar (2022) studied the clinically relevant features for diagnosing PD based on gait analysis and examined the efficacy of several ML models including SVM, KNN, DT and RF. Identifying the optimal spatiotemporal features through recursive feature elimination technique, they devised a decision support system which exploited the age-gender information to predict the PD severity level. However, their work failed to consider the imbalanced dataset, which may significantly affect the performance of the classifier model. Beigi et al. (2023) studied not only the diagnosis of PD based on the gait impairment analysis but also the efficacy of medication on the subjects. Extracting time, energy and statistical features to train the ML models, they achieved the highest classification accuracy of 99% using decision tree algorithm. In another interesting study, Shuzan et al. (2023) investigated the potential of ML models to classify the gait impairments using KNN model, trained using the time domain and wavelet features. Nevertheless, the major limitation of the aforementioned approaches is that the manual engineering of the gait features which may result in the possibility of few of the prominent ones being ignored. Likewise, several previous studies investigated the ML-based PD diagnosis, which utilised hand-crafted features.

As is well known, the hand-crafted features are subjective to the type of classifier design and may result in high computation time in the case of redundant features. Moreover, there have been attempts in the literature to design a CNN-based classifier models for PD diagnosis. However, many of the CNN-based techniques utilised only convolution operation to downsample the high-dimensional feature map and failed to explore the important gait characteristics based on decomposition techniques. Hence, the major focal point of this paper is to develop a decision support framework which integrates a VMD technique with the DCNN model to mine the prominent gait features for implementing multi-class severity prediction of PD.

3. Dataset description

This study has utilised the publicly available gait pattern from Physionet for diagnosing the stages of PD (PD: P.D.D., 2020). The database, collected at the Gait & Neurodynamics Laboratory, Tel-Aviv Sourasky medical centre, Israel, contains the PD severity score based on UPDRS and H&Y scale. Table 1 gives the demographic data including the age, height and weights of the subjects who volunteered for gait recording. For data acquisition, 8 foot worn sensors, as illustrated in Figure 1, were located in the insole of each foot and the VGRF signal was recorded when the subjects walked for 2 minutes. The 16 VGRF time series data were acquired at a sampling rate of 100 Hz. The VGRF signals were recorded for three different walking tests and the details are as follows. To assess the treadmill walking on gait rhythmicity and gait variability, Frenkel-Toledo et al. (2005) acquired the gait pattern using

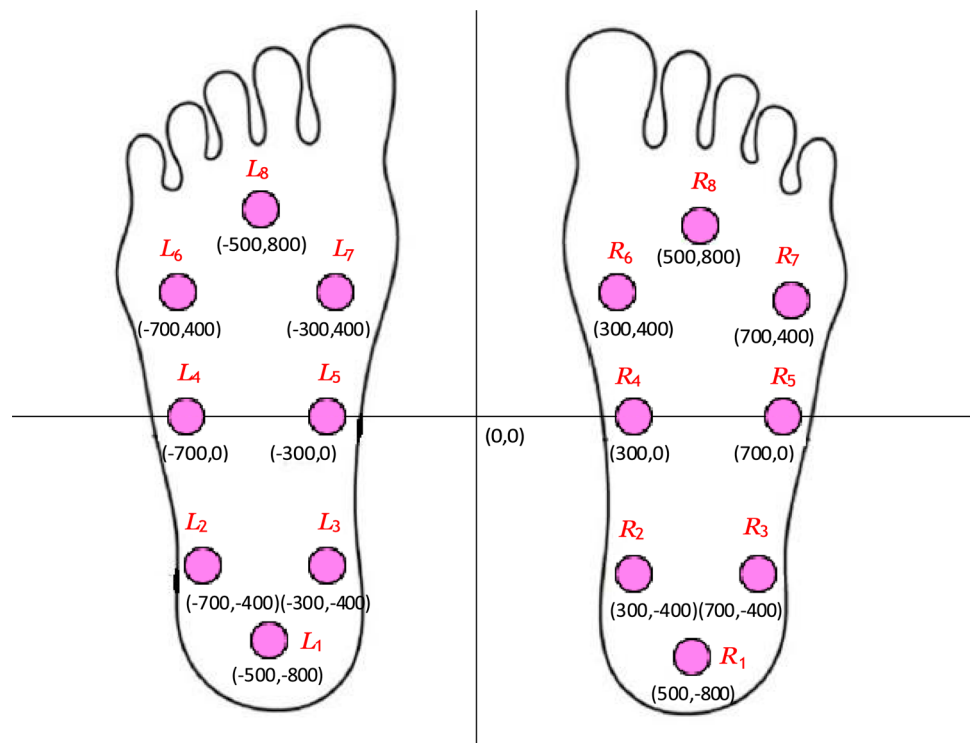


Figure 1. Position of VGRF sensors in each foot.

the foot worn sensors from 35 PD patients with a H&Y scale 2–2.5 and 29 healthy controls. Similarly, to study the effect of rhythmic auditory stimulation (RAS) on spatiotemporal measures and stride and swing variability, Hausdorff et al. (2007) contributed gait patterns from 26 healthy controls and 29 PD patients with H&Y stage 2, 2.5 and 3. One of the key aspects of this dataset is that it clearly demonstrates the effect of stride time variability of PD patients and covers stages from mild to moderate severity. In another walking test, for examining the relationship between the cognitive function and gait, Yogev et al. (2005) examined the effects of dual tasking on gait for different conditions ranging from simple task to attention demanding task. Patients who were taking antiparkinsonian medications were invited to participate in the gait acquisition process and their gait patterns were recorded when the subjects walked at a comfortable pace on a 25 m long, 2 m wide corridor while performing dual task. For easy reference, the three gait datasets will be hereafter referred to as Toledo (Si) (Frenkel-Toledo et al., 2005), Hausdorff (Ju) (Hausdorff et al., 2007) and Yogev (Ga) (Yogev et al., 2005). Table 2 presents the number of subjects along with their PD stages according to H&Y scale in each dataset. Figure 2, which shows the exemplary VGRF signals of both healthy and PD patients, manifests that compared to healthy subjects, the PD patients exert only half of the foot plantar pressure while walking. Moreover, the number of gait cycles of healthy control is more than that of the PD patients. Hence, the step time, stride time, cadence and stride interval are more in case of the healthy subjects compared to PD patients.

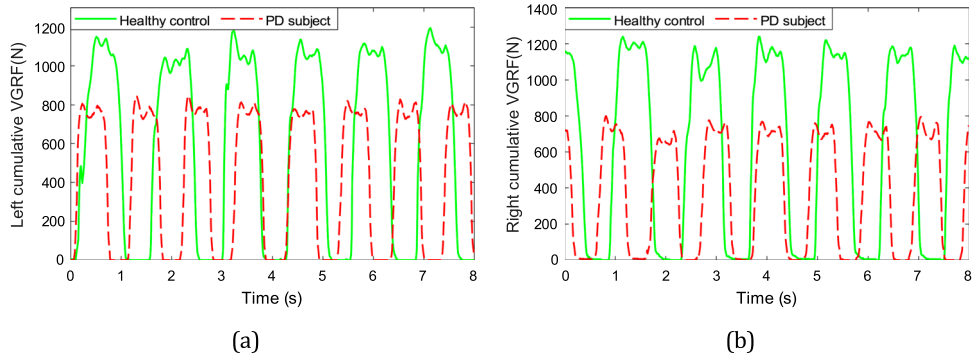


Figure 2. Representative VGRF signals (a) Left foot sensors (b) Right foot sensors.

Table 1. Demographics of PD and healthy controls volunteered for the walking tests.

Dataset	Category	Female	Male	Weight (Kg)	Height (m)	Age (Yrs) (Yrs)
Yogev (Ga)	Healthy	8	10	74.3 ± 12.8	1.67 ± .09	57.7 ± 6.6
	PD Patient	9	20	73.2 ± 11.1	1.68 ± .08	61.7 ± 8.7
Hausdorff (Ju)	Healthy	14	12	66.7 ± 11.08	1.83 ± .07	39.4 ± 18.4
	PD Patient	13	16	75.2 ± 16.9	1.86 ± .16	66.81 ± 10.8
Toledo (Si)	Healthy	11	18	71.7 ± 11.01	1.69 ± .07	64.6 ± 6.9
	PD Patient	13	22	70.4 ± 8.5	1.65 ± .08	67.3 ± 9.2

Table 2. Ground truth of number of severity and healthy subjects in three datasets (S-Severity ;H-Healthy).

Dataset	S-3	S-2.5	S-2	H
Yogev (Ga)	6	8	15	18
Hausdorff (Ju)	4	13	12	26
Toledo (Si)	0	6	29	29

4. Methodology

Figure 3 shows the proposed VMD-RP-DCNN architecture for discriminating the stride variability which can help to classify the stages of PD. The VGRF time series dataset is initially preprocessed to remove the outliers and filtered using median filter to minimise the effect of VGRF sensor noise in gait signals. The preprocessed VGRF signals are decomposed using the VMD technique majorly for two reasons: (1) to denoise and (2) to split the raw gait data into IMFs ranging from high frequency to low frequency. Subsequently, through spectral separation of the decomposed signals, the prominent IMFs that contain the highest power content have been identified and utilised to formulate the RP images that can be fed to train the DCNN classifier. The DCNN consists of an alternate convolution and pooling layers which are used to identify the cardinal features from the recurrence images and down-sample the feature map, respectively. Then, the fully connected layer organises the feature vector and feeds to softmax layer to predict the class label (PD severity) of the input signal based on the probabilistic function. In the following sections, we briefly discuss the VMD technique applied to decompose the VGRF signal and the approach followed to convert

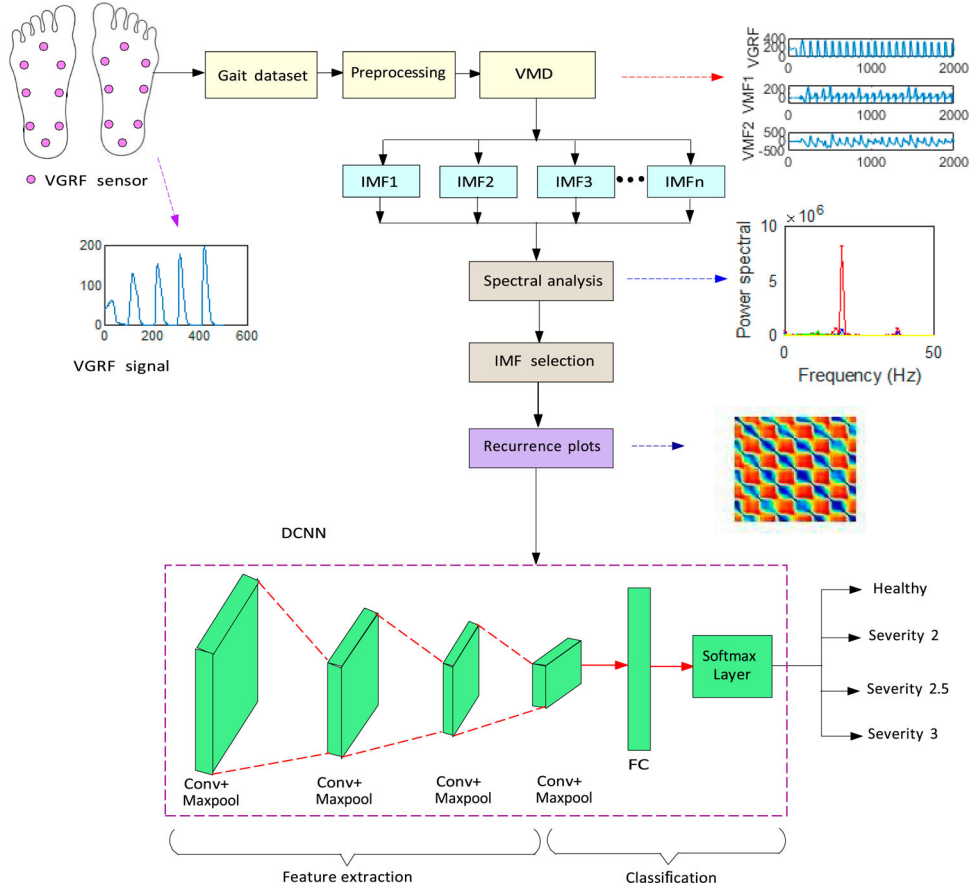


Figure 3. Proposed VMD-RP-DCNN framework for PD severity prediction based on gait analysis.

the IMFs into RP images to enhance the multi-class PD severity prediction performance of DCNN classifier.

4.1. VMD

VMD is an adaptive and non-recursive decomposition technique which is highly suitable for nonlinear and non-stationary signals. Compared to empirical mode decomposition (EMD) technique, which lacks strong mathematical theory, VMD is founded on Wiener filtering and Hilbert transform. Moreover, EMD is sensitive to noise and suffers from mode mixing problems. However, VMD extends the Wiener filtering to multiple adaptive bands and is less sensitive to noise compared to EMD. VMD decomposes an input signal s into multiple IMFs and the superposition of the IMFs will result in the input signal s as described in Equation (1).

$$s = \bar{s} + \delta \quad (1)$$

where \bar{s} and δ represent the original signal and noise signal, respectively. Each IMF has a centre frequency f_k and is band limited. Hence, the IMF can be described as amplitude-modulated-frequency-modulated (AM-FM) signals as follows.

$$u_k = A_k \cos(\phi_k) \quad (2)$$

where A_k and ϕ_k are the non-negative envelopes and non-decreasing phases. The VMD estimates N appropriate IMFs $u_1(t), u_2(t), \dots, u_N(t)$ with their respective centre frequencies w_1, w_2, \dots, w_N . The decomposition approach is formulated as follows.

$$\begin{aligned} \min_{\{u_k\}, \{w_k\}} \quad & \left\{ \sum_{k=1}^K \left\| \partial_t \left[\left(\delta(t) + \frac{j}{\pi t} \right) * u_k(t) \right] e^{-jw_k t} \right\|_2^2 \right\} \\ \text{s.t.} \quad & \sum_K u_k = s \end{aligned} \quad (3)$$

Firstly, through Hilbert transform the analytical signal of every subsignal (mode) is computed to get the unilateral spectrum. Secondly, to alter the estimated centre frequency, an exponential term is augmented with the unilateral spectrum of each mode. Finally, the bandwidth of the each IMF (mode) is obtained through gradient squared $L2$ norm. To recast the constrained problem into an unconstrained optimisation problem, the Lagrangian multipliers and quadratic penalty are augmented as follows.

$$\begin{aligned} L(\{u_k\}, \{w_k\}, \lambda) = \alpha \sum_{k=1}^K & \left\| \partial_t \left[\left(\delta(t) + \frac{j}{\pi t} \right) * u_k(t) \right] e^{-jw_k t} \right\|_2^2 \\ & + \left\| f(t) - \sum_{k=1}^N u_k(t) \right\|_2^2 + \left\langle \lambda(t), f(t) - \sum_{k=1}^N u_k(t) \right\rangle \end{aligned} \quad (4)$$

where α and λ are the regularisation factor and Lagrangian multiplier, respectively. To solve the variational problem and determine the saddle point, the alternate direction method of multiplier (ADMM) is used. Then, the extracted modes along with their corresponding centre frequencies are alternately updated in spectral domain as follows.

$$\hat{u}_k^{n+1}(\omega) = \frac{\hat{f}(\omega) - \sum_{i \neq k} \hat{u}_i(\omega) + \frac{\hat{\lambda}(\omega)}{2}}{1 + 2\alpha (\omega - \omega_k)^2} \quad (5)$$

$$\omega_k^{n+1} = \frac{\int_0^\infty \omega |\hat{u}_k(\omega)|^2 d\omega}{\int_0^\infty |\hat{u}_k(\omega)|^2 d\omega} \quad (6)$$

Subsequently, the Lagrangian multiplier is updated as follows.

$$\hat{\lambda}^{n+1}(\omega) \leftarrow \hat{\lambda}^n(\omega) + \tau \left(\hat{f}(\omega) - \sum_k \hat{u}_k^{n+1}(\omega) \right) \quad (7)$$

where τ indicates the noise tolerance of VMD. The convergence condition for VMD is as follows.

$$\frac{\sum_k \left\| \hat{u}_k^{n+1} - \hat{u}_k^n \right\|_2^2}{\left\| \hat{u}_k^n \right\|_2^2} < \epsilon \quad (8)$$

4.2. Recurrence plots

Recurrence plots (RP), put forward by Eckmann and his team (Eckmann et al., 1995), is a visualisation tool that can be used for nonlinear analysis of time series data and extract visual features for examining the recurrence characteristics (Shankar et al., 2021). Particularly, the recurrence plots can be used for investigating the intrinsic similarity and smoothness of a time series data. Computing the distances between the states in phase space, the RP can encode the time series as 2D images. Since RP takes the recurrence nature in time series including chaotic behaviour and nonlinearity, it helps to explore the correlations in pattern, structural changes and predictive features in time series data graphically over a time period (Hou et al., 2022). In this work, we utilise the recurrence plots to map the prominent frequency modes of 1D VGRF time series signals into the image domain and improve the possibility of extracting invisible features of the 1D signals. Algorithm 1 presents the pseudo code for transforming the decomposed 1D VGRF signals into recurrence plots.

Algorithm 1 Pseudo code-Recurrence plot

Input: Decomposed VGRF signals (IMF1, IMF2..IMFn)

Output: Recurrence plots (RP)

Step 1: Embed time series data (IMFs) into m-dimensional space

$$X_i = (x_i, x_{i+\tau}, x_{i+2\tau}, \dots, x_{i+(m-1)\tau})$$

where m and τ represent embedding dimension and time delay, respectively.

Step 2: Calculate the distance D_{ij} between any two observed subsequences.

$$D_{ij} = \|x_i - x_j\|$$

Step 3: Determine the recurrence matrix R_{ij} .

$$R_{ij} = \Theta(\epsilon - D_{ij})$$

where ϵ is the threshold for closeness and Θ is the Heaviside function defined as follows.

$$\Theta(x) = \begin{cases} 0 & \text{amp;} x < 0 \\ 1 & \text{amp;} x \geq 0 \end{cases}$$

Step 4: Obtain the modal components from the decomposition and form the RP.

4.3. DCNN classifier model

DCNN, which derives a biological inspiration from the visual cortex, is a deep feed-forward artificial neural networks (El Maachi et al., 2020; Fawaz et al., 2019). To address the two fundamental limitations of shallow networks including large number of hyperparameters tuning and negligence of correlation among activation maps, DCNN was put forward with two interesting features: sparse connectivity and weight sharing (Camps et al., 2018). In this work, exploiting the potential of theses features, we present a DCNN model for extracting the hidden biomarkers from gait pattern for effective severity prediction of PD. The DCNN has four types of layers namely convolution, pooling, fully connected and softmax.

4.3.1. Convolutional layer

It consists of a group of filters that slide over the input data according to the kernel function to capture the significant attributes. The input is convolved with the kernel function based

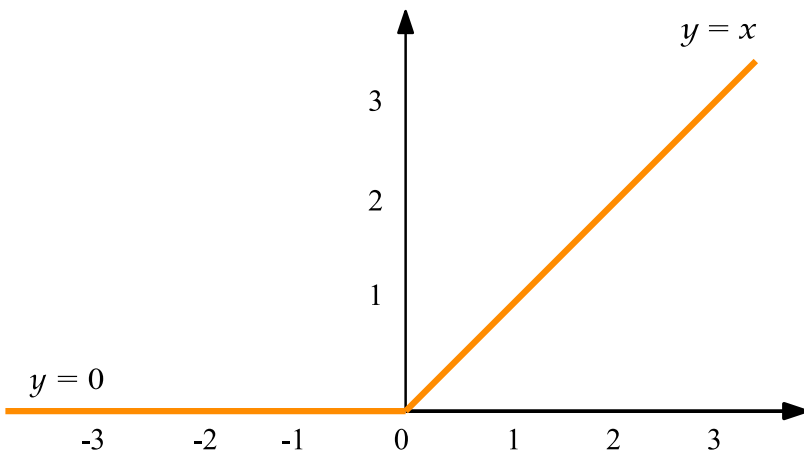


Figure 4. ReLU activation function.

on the following equation.

$$c_m = \sum_{n=0}^{P-1} f_n k_{m-n} \quad (9)$$

where k , c , P and f indicate input signal, convolved output, data samples and filter, respectively. When n varies from 0 to $P-1$, the filter function f_n is convolved with the input signal. After the convolution operation, the convolved matrix is given to the rectified linear unit (ReLU) activation function to account for nonlinearities in time series data. ReLU, as illustrated in Figure 4, is a class of nonlinear activation function which basically outputs zero when it receives a non-positive value and the value itself in any other case. ReLU does not saturate and is computationally very efficient (Arifoglu & Bouchachia, 2019). Moreover, it converges faster than other nonlinear thresholding functions like *sigmoid/tanh*. The mathematical representation of ReLU is as follows.

$$\text{ReLU}(z) = \max(0, z) = \begin{cases} z & z > 0 \\ 0 & z \leq 0 \end{cases} \quad (10)$$

4.3.2. Pooling layer

The feature map obtained from the nonlinear threshold function passes through the pooling layer to downsample the feature map/activation map and extract the most representative features. Basically, the pooling layer minimises the number of parameters to be learnt and the computations to be performed in the network (He et al., 2020). Providing a summary statistic of nearby outputs, pooling layer majorly performs dimensionality reduction and guarantees translation invariance. The hyperparameters of pooling layer are filter size (f_s), stride window (s) and type of pooling, which are commonly either max pooling or average pooling.

4.3.3. Fully connected (FC) layer

It creates a connection from one layer to the next layer through weighted input matrix augmented with a bias vector. In general, the DCNN process is classified into two major groups

namely feature extraction and classification (Basha et al., 2020). The convolution layer along with the pooling layer is responsible for feature extraction and the fully connected layer and softmax layer handle the decision making process (San-Segundo et al., 2019). The resultant output activation function map is flattened into a single column vector, and fed as an input to the FC layer. The output of the nodes in FC layer is determined as follows.

$$x_i = b_i + \sum_j \omega_{ji} y_j \quad (11)$$

where ω indicates the weights and b represents the bias vector. x and y are the output of the respective current and previous layers. Subsequently, the output from the FC layer is given to softmax layer to predict the classes.

4.3.4. Softmax layer

It converts the class scores from FC layer into a probability mass function (Xia et al., 2018). Taking a vector of K -dimensional real-valued score z , the softmax function in (12) converts it to a K -dimensional vector of $f(z)$ with values ranging from 0 to 1.

$$f_j(z) = \frac{e^{z_j}}{\sum_{j=1}^K e^{z_k}} \quad (12)$$

$$H_{p'}(p) = - \sum_i p'_i \log(p_i) \quad (13)$$

$$p_i \in (0, 1) : \sum_i p_i = 1 \forall i \quad (14)$$

where p represent the estimated probability distribution, p' is the true distribution and i indicates the different classes. For the multi-class classification, the softmax layer utilises the categorical cross entropy function given (13). To prevent overfitting in DCNN training, the L_2 regularisation technique, which is also called ridge regression, is used. Equation (15) represents the regularised objective function.

$$\hat{L}(X, \omega) = L(X, \omega) + \lambda R(\omega) = L(X, \omega) + \lambda \sum_i |\omega_i|^2 \quad (15)$$

where λ is the regularisation strength, which adjusts the relative contribution of the norm penalty term $R(\omega)$ with respect to the standard loss function $L(w, X)$. The augmented loss function will be convex because the penalty term $R(\omega)$ is convex (Acharya et al., 2018; Arcos-García et al., 2018; Saba et al., 2019).

4.4. Adam optimiser

For minimising the loss function in the DCNN, this study utilises an Adam optimiser, which not only requires less memory for implementation but also offers computationally effective approach. Adam, which combines the heuristics of RMSProp (root mean square propagation) and momentum techniques, is a widely used first-order stochastic optimisation algorithm to train the DNNs. Adam, the name coined by the author from “adaptive moment estimation”, is an alternate for the stochastic gradient descent technique to update the

weights of DNNs. Moreover, it is highly suited for solving the problems with sparse gradients. Therefore, Adam optimisation is largely used in several deep learning optimisation problems. The pseudo code of Adam optimiser is presented in Algorithm 2.

The core idea behind the algorithm is as follows. Estimating the 1st and 2nd moments of the gradient, the algorithm adapts the learning rate for the weight of neural network. The 1st and 2nd moments which are mean and the uncentred variance are computed using the following equations.

$$m_t = \gamma_1 \cdot m_{t-1} + (1 - \gamma_1) \cdot g_t \quad (16)$$

$$v_t = \gamma_2 \cdot v_{t-1} + (1 - \gamma_2) \cdot g_t^2 \quad (17)$$

where m_t and v_t represent the estimates of 1st and 2nd moment gradients, respectively. As the optimisation process starts with m_t and v_t being initialised as null vectors, to correct the bias in estimation, the moments are updated as follows.

$$\hat{m}_t = m_t / (1 - \gamma_1^t) \quad (18)$$

$$\hat{v}_t = v_t / (1 - \gamma_2^t) \quad (19)$$

Subsequently, the Adam update rule is utilised to update the weights.

$$\theta_t = \theta_{t-1} - \alpha \cdot \hat{m}_t / (\sqrt{\hat{v}_t} + \epsilon) \quad (20)$$

Algorithm 2 Pseudo code-Adam optimiser

- 1: Set the step size α , hyper parameters $\gamma_1, \gamma_2 \in [0, 1]$, stochastic cost function $f(\theta)$ with parameters θ
- 2: Initialise the parameter vector θ and time step $t = 1, \dots, T$
- 3: Initialise the 1st and 2nd moment vectors: $m_0 = 0, v_0 = 0$
- 4: **while** until θ_t has converged **do**
- 5: $i = i + 1$
- 6: Determine the gradients $g_t = \Delta_\theta f_t(\theta_{t-1})$
- 7: Compute the 1st and 2nd raw moment estimates

$$m_t = \gamma_1 \cdot m_{t-1} + (1 - \gamma_1) \cdot g_t$$

$$v_t = \gamma_2 \cdot v_{t-1} + (1 - \gamma_2) \cdot g_t^2$$
- 8: Estimate the bias corrected 1st and 2nd moment estimates

$$\hat{m}_t = m_t / (1 - \gamma_1^t)$$

$$\hat{v}_t = v_t / (1 - \gamma_2^t)$$
- 9: Perform parameters update $\theta_t = \theta_{t-1} - \alpha \cdot \hat{m}_t / (\sqrt{\hat{v}_t} + \epsilon)$
- 10: Return θ_t
- 11: **end while**

4.5. Classifier performance metrics

The performance of the proposed DCNN classifier model is assessed using the following performance measures: accuracy, sensitivity, precision, specificity, F-score and Mathew's

correlation coefficient (MCC). Accuracy (Acc) is the ratio of number of correct predictions to the total number of predictions.

$$\text{Acc} (\%) = \frac{TN + TP}{TN + TP + FN + FP} * 100\% \quad (21)$$

where FP, FN, TP and TN are false positive, false negative, true positive and true negative, respectively.

Sensitivity (Sen), which is also called recall, indicates the correctly classified predictions to the total number of positive samples.

$$\text{Sen} (\%) = \frac{TP}{TP + FN} \times 100\% \quad (22)$$

Specificity (Spe), also referred to as true negative rate (TNR), is the ratio of correctly identified negative predictions to the total number of negative samples. Therefore, the sensitivity denotes how correctly the classifier predicted the positive samples and similarly, the specificity indicates the ability of the classifier to predict the negative samples.

$$\text{Spe} (\%) = \frac{TN}{TN + FP} \times 100\% \quad (23)$$

Positive prediction value (PPV), also called precision, reflects the ratio of positive samples to the total number of positive predicted samples.

$$\text{PPV} (\%) = \frac{TP}{TP + FP} \times 100\% \quad (24)$$

F-score, which is the weighted harmonic mean of recall and precision, is a common classifier metric, ranging from 0 (representing the worst performance) to 1 (indicating the best performance).

$$\text{F-score} (\%) = 2 \times \frac{\text{Precision} \times \text{Recall}}{\text{Precision} + \text{Recall}} \times 100\% \quad (25)$$

MCC manifests the correlation between the actual and predicted classifications. It ranges from $+1$ to -1 . A perfect prediction takes a value of $+1$ and total disagreement between true values and prediction assumes -1 .

$$\text{MCC} = \frac{TN \times TP - FN \times FP}{\sqrt{(FP + TP)(FP + TN)(TP + FN)(FN + TN)}} \quad (26)$$

5. Experimental results and discussion

This study utilises the VGRF dataset of 93 PD subjects and 73 healthy controls from three walking tests to test the efficacy of the proposed approach. The proposed VMD-RP-DCNN framework is implemented using Keras library on a hardware platform with Intel core-i7, 64 GB RAM and Nvidia GeForce 16 GB GPU. Each gait sample contains 18 columns of data which include the 16 VGRF sensor signals along with 2 cumulative values from each foot. Firstly, to remove the gait initiation and termination effects, the data samples of 20s in the beginning and 10s at the end are removed. The datasets Ga (Frenkel-Toledo et al., 2005), Ju (Hausdorff et al., 2007) and Si (Yogev et al., 2005) contain sample size of about 13,500,

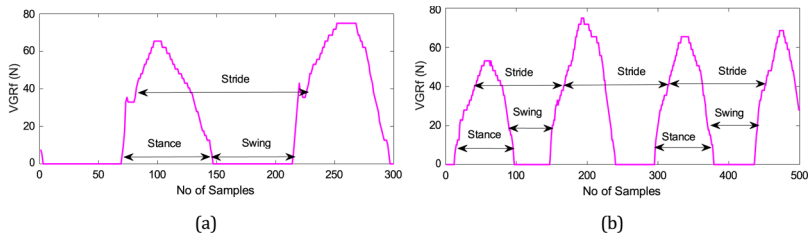
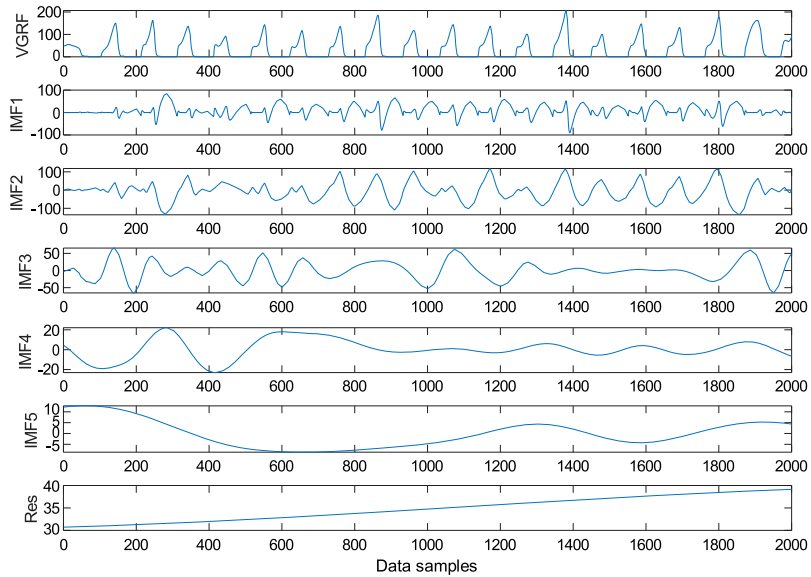


Figure 5. VGRF times series plot with frame size (a) 300×1 (F_1) (b) 500×1 (F_2).

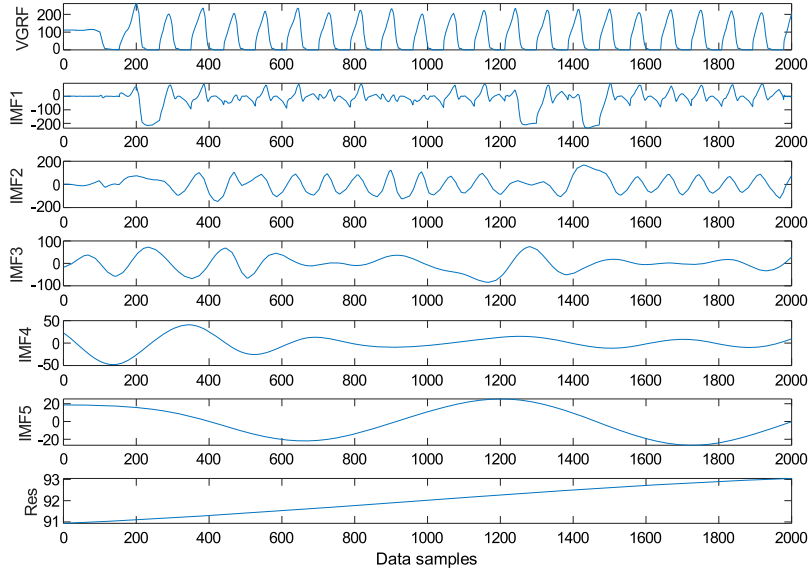
11,730, and 7700, respectively for each subject. Hence, the total data samples available for training the deep learning model is roughly 2,241,000 data points. However, as each dataset has different sample size, to make them of equal length, the datasets are divided into input segments of 300 and 500 frames. Secondly, two input frames 300×1 (F_1) and 500×1 (F_2) are considered to assess the impact of the input frame size on the classifier performance. Figure 5 illustrates the VGRF input data for 300 and 500 data samples. It is worth noting that the VGRF plot is the signal acquired from one of the 16 sensors. Figure 5(a) manifests that the gait cycle comprises one stride phase and swing phase. However, Figure 5(b) that corresponds to F_2 input frame consists of two swing phases and two stride to stride variabilities. Hence, the larger input frame contains more kinematic features that can assist the deep learning network to identify the prominent biomarkers during the training phase. After dividing the dataset into equal segments, the selected input frames of VGRF signals are decomposed using the VMD technique to denoise the VGRF signals and split the raw signal into low and high frequency IMFs. Figure 6 illustrates the exemplary five level decomposition of VGRF signals of both healthy and PD subjects.

Figure 7 depicts the sample 3D plot of the decomposed signal, which highlights that the VMD technique can concurrently decompose the VGRF signal into group of narrow-band modes and minimise spectral overlapping. As the first level IMF contains the high frequency component, to remove the noise in the raw signal, all the IMFs, excluding the first level IMF, have been summed up to reconstruct the original VGRF signal. Figure 8 shows the reconstructed VGRF signal from the IMFs and we can notice that VMD assures signal integrity. Thus, VMD technique helps to not only denoise the signal but also extract robust gait features. Subsequently, to select the prominent IMFs that contain the discriminative features, the PSD of each IMF is calculated. Figure 9 shows the representative PSD of each IMF for L_2 sensor. We can observe from the PSD plots that among all the decomposed modes, IMF2 and IMF3 contain significant power content. Hence, the IMF2 and IMF3 are identified to be prominent modes and are used to generate the RP images.

Figure 10 illustrates the exemplary recurrent images of the dominant IMFs for the four output classes (H,S-2, S-2.5 and S-3). We can note that the RP, encoding the time series data as 2D images, manifests the structural changes in IMFs of the healthy and PD subjects and helps to analyse the periodic nature in the four classes from time series data. Consequently, we utilise the RP to map the 1D VGRF time series signals into the image domain and improve the possibility of extracting invisible features of the 1D signals, leading to enhanced PD severity prediction capability of DCNN model.



(a)



(b)

Figure 6. Representative original VGRF signal from Ga dataset for L3 sensor and decomposed IMFs with residual based on VMD for (a) Heathy (b) PD severity level 2.5 (S-2.5).

Table 3 gives the configuration parameters of the proposed DCNN framework, which contains 4 convolutional layers, 4 average pooling layers, 2 fully connected layers and a softmax layer. Intermediate layers utilise ReLU as an activation function because ReLU results in reduced likelihood of the gradient vanishing. In fully connected layer, 50 input and 4 output

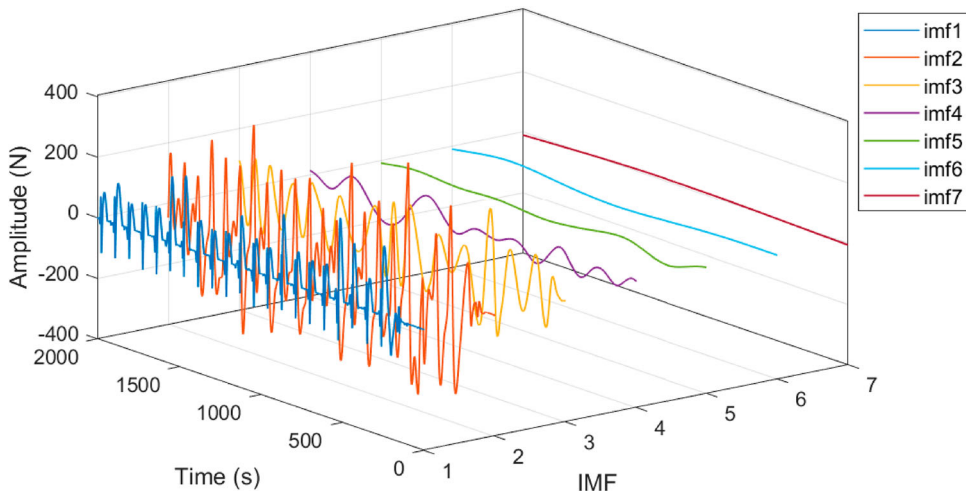


Figure 7. Representative 3D plot depicting the decomposed IMFs from Ga dataset for severity level S-2.5.

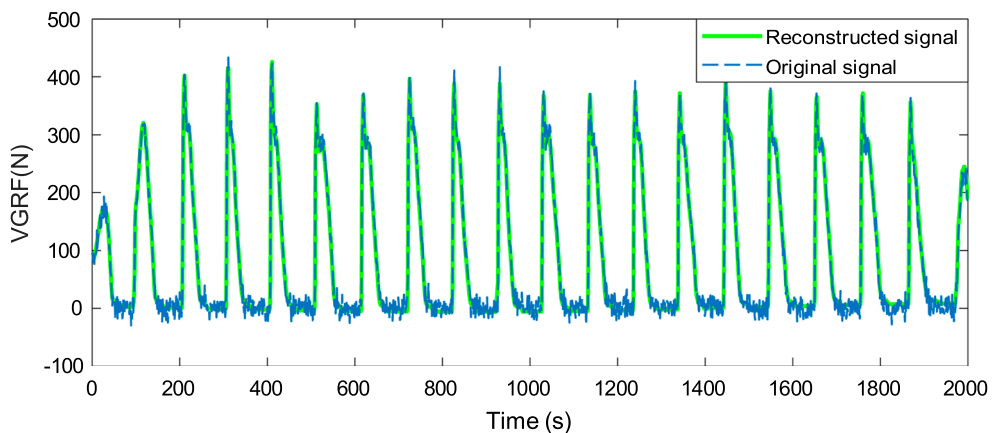


Figure 8. Signal reconstruction using VMD.

layers are configured based on the three classes of PD. The filter size for the four convolutional layers are 12, 24, 48 and 96 and for the fully connected layer the filter size is chosen to be 50. The kernel functions in the convolutional layer have a stride window of (1,1). For dimensionality reduction and extracting the key features in the pooling layer, the stride window of (2,2) is used. To regularise the network during training, some neurons from the fully connected layers are dropped randomly for each mini-batch, thereby enabling the classifier to learn from a small group of input features rather than using the entire input feature set.

For minimising the loss function, the configuration of hyper parameters of Adam optimiser is as follows: the decay rates $\beta_1 = 0.9$, $\beta_2 = 0.99$, the learning rate $\alpha = 0.001$, the threshold $\delta = 10^{-5}$ and constant $\epsilon = 10^{-8}$. To maintain optimality between learning rate and network training error, Adam follows the adaptive learning rate approach and finds the optimal weights of the network. To minimise the data overfitting, L_2 regularisation

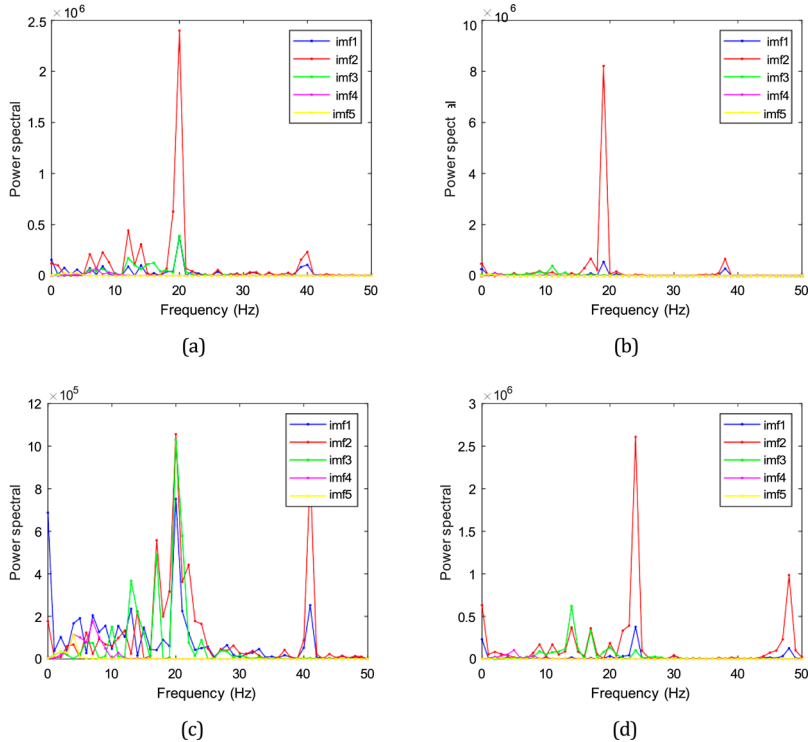


Figure 9. Representative power spectral plot from Ga dataset for L3 sensor (a) H (b) S-2 (c) S-2.5 (d) S-3.

Table 3. VMD-RP-DCNN configuration.

Layers	Activation	Filter	Stride	Parameters
Conv1	ReLU	12	(1,1)	48
Max-Pooling	–	2	(2,2)	0
Conv2	ReLU	24	(1,1)	888
Max-Pooling	–	2	(2,2)	0
Conv3	ReLU	48	(1,1)	3504
Max-Pooling	–	2	(2,2)	0
Conv4	ReLU	96	(1,1)	13,920
Max-Pooling	–	2	(2,2)	0
Fully connected	ReLU	100	–	86,450
Fully connected output	Softmax	4	–	36

technique is used, and the softmax layer is employed to normalise the DCNN outputs. For validation, the gait dataset is divided into 80% and 20% for training and testing, respectively. For validation, the performance of the proposed approach is compared with that of the VDCNN trained using the raw VGRF signals with similar parameter configurations as given in Table 3.

5.1. Performance evaluation

Figures 11 and 12 show the confusion matrix of VDCNN and the VMD-RP-DCNN classifier models for the two input frames (F_1 and F_2). The VDCNN with F_1 input frame, illustrated

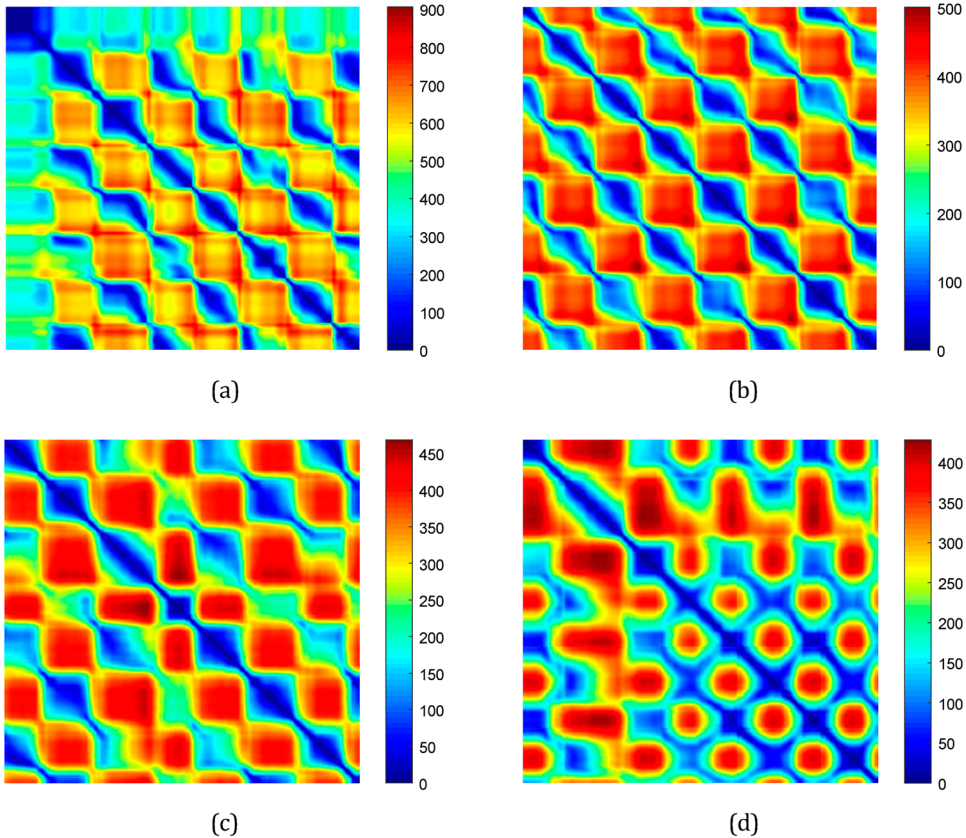


Figure 10. Exemplary recurrence plots of decomposed VGRF signals of (a) Healthy (b) Severity-2 (c) Severity-2.5 (d) Severity-3.

in Figure 11(a), predicts the “healthy” class with an accuracy of 94.3 whereas the proposed DCNN framework with F_1 input frame, shown in Figure 12(a), predicts the same class with the accuracy of 97.25. Moreover, we can also note that the proposed VMD-RP-DCNN framework offers better classification accuracy for the PD classes (S2–S3) compared to the performance of VDCNN. Hence, to further quantify the classifiers performances, six metrics used for objective performance comparison are given in Table 4. The specificity of all the PD classes in the case of the proposed approach is higher than that of similar classes in VDCNN. Thus, the VMD-RP-DCNN has demonstrated that it can effectively exclude the patients without the disease being recognised as PD. Likewise, it can also be noted that the F-score is relatively same among the classes, which corroborates that the proposed approach is relatively consistent in predicting the classes.

Figures 13 and 14 show the respective accuracy plots of the VDCNN and the proposed classifier scheme. It is evident from Figure 14(b) that the proposed approach minimises the overfitting significantly in case of F_2 input frame. The primary reason for the improvement in the testing performance can be attributed to the L2 regularisation technique used to address the overfitting issue. Moreover, from Figures 15 and 16 that illustrate the loss function plots of the classifier models, we can observe that the VMD-RP-DCNN with F_2 frame has

Figure 11 consists of two confusion matrices, (a) and (b), for the VDCNN model. Both matrices have 'True label' on the y-axis and 'Predicted label' on the x-axis, with four categories: H, S-2, S-2.5, and S-3.

(a) F1 confusion matrix:

	H	S-2	S-2.5	S-3
H	94.30	5.67	4.74	3.40
S-2	3.92	91.20	5.99	5.74
S-2.5	1.52	2.66	88.18	2.90
S-3	0.26	0.47	1.09	87.96

(b) F2 confusion matrix:

	H	S-2	S-2.5	S-3
H	93.31	1.92		
S-2	2.6	95.92	1.81	3.37
S-2.5	2.42	0.48	98.19	1.12
S-3	1.67	1.68		95.51

Figure 11. Confusion matrix – VDCNN (a) F1 (b) F2.

Figure 12 consists of two confusion matrices, (a) and (b), for the VMD-RP-DCNN model. Both matrices have 'True label' on the y-axis and 'Predicted label' on the x-axis, with four categories: H, S-2, S-2.5, and S-3.

(a) F1 confusion matrix:

	H	S-2	S-2.5	S-3
H	97.25	1.72	0.69	0.34
S-2	1.98	97.22	0.40	0.40
S-2.5	2.75	1.83	95.42	
S-3	2.17	2.17		95.66

(b) F2 confusion matrix:

	H	S-2	S-2.5	S-3
H	99.89	0.26		0.17
S-2	0.03	99.68	0.35	1.18
S-2.5		0.06	99.43	
S-3	0.08		0.22	98.65

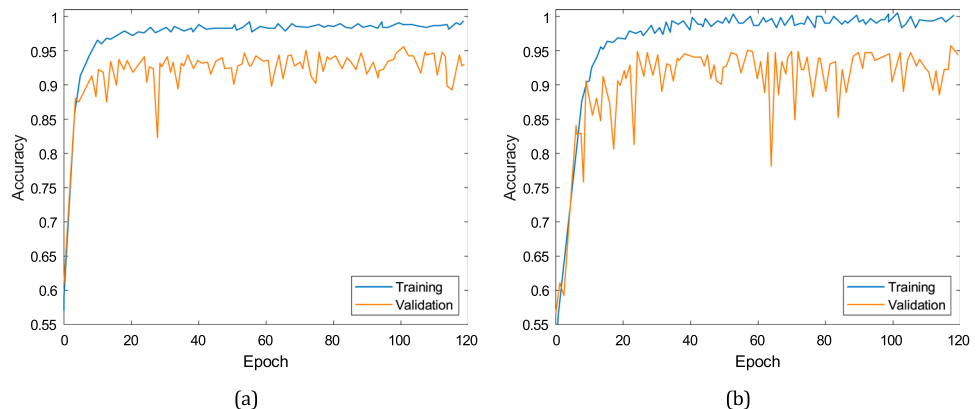
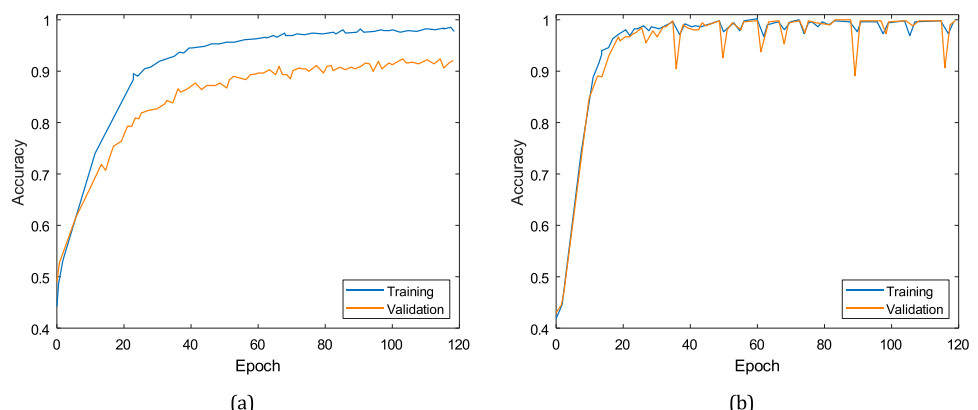
Figure 12. Confusion matrix – VMD-RP-DCNN (a) F1 (b) F2.

less loss function value of 0.061 compared to similar frame in VDCNN that has the loss function value of 0.592. Hence, these performance metrics substantiate that the performance of proposed scheme, which utilises the RP images of dominant VGRF modes, is significantly better than that of the VDCNN that utilises the raw VGRF times series signal for classification.

To assess the performance of the VMD-RP-DCNN in classifying the three stages of PD, the statistical distribution of the performance metrics across different classes is computed. Figure 17 illustrates the statistical distribution of three key performance metrics such as sensitivity, accuracy and specificity as a box plot for all four classes of both VDCNN and VMD-RP-DCNN classifier models. Compared to VDCNN with *F2* input frame that has the average classification accuracy of 96.02%, the proposed DCNN with *F2* input frame offers better accuracy of 98.45%. Similarly, the sensitivity of the proposed scheme across the classes is

Table 4. Classification performance metrics for VDCNN and VMD-RP-DCNN.

Classifier	Frame	Class	Acc(%)	Sen(%)	Spe(%)	PPV(%)	F-score	MCC
VCNN	F1	H	96.31	98.43	94.73	93.31	0.95	0.93
		S-2	96.88	95.23	97.78	95.91	0.96	0.93
		S-2.5	98.37	91.06	99.69	98.19	0.94	0.94
		S-3	98.29	84.16	99.63	95.51	0.891	0.91
	F2	H	94.48	93.12	95.55	94.30	0.93	0.89
		S-2	93.82	90.97	95.33	91.19	0.91	0.86
		S-2.5	96.12	89.23	97.54	88.18	0.87	0.86
		S-3	98.57	93.44	98.98	87.96	0.90	0.89
VMD-RP-DCNN	F1	H	96.69	97.01	96.45	95.41	0.96	0.93
		S-2	97.39	95.55	98.42	97.12	0.96	0.94
		S-2.5	98.53	95.10	99.13	95.41	0.95	0.95
		S-3	99.55	95.24	99.84	97.56	0.96	0.96
	F2	H	97.55	97.24	97.77	96.91	0.97	0.95
		S-2	97.83	97.23	98.17	96.85	0.97	0.95
		S-2.5	98.83	95.41	99.48	97.19	0.96	0.96
		S-3	99.41	95.65	99.68	95.65	0.95	0.95

**Figure 13.** Accuracy plot of VDCNN (a) F1 (b) F2.**Figure 14.** Accuracy plot of VMD-RP-DCNN (a) F1 (b) F2.

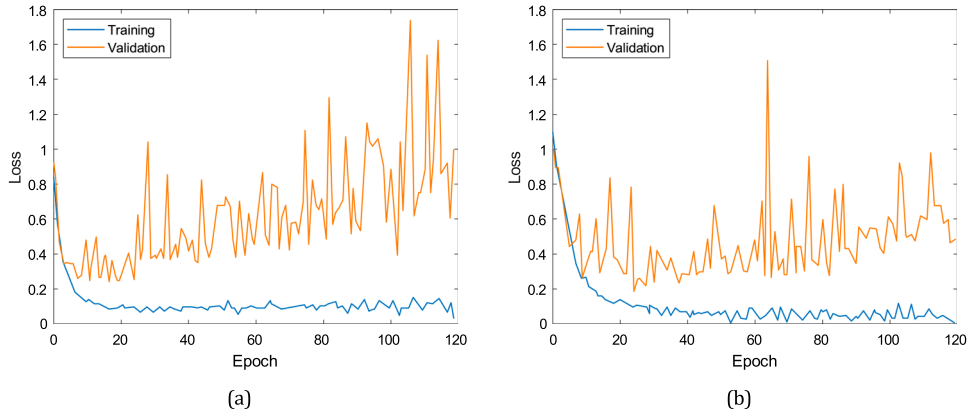


Figure 15. Loss function plot of VDCNN (a) F1 (b) F2.

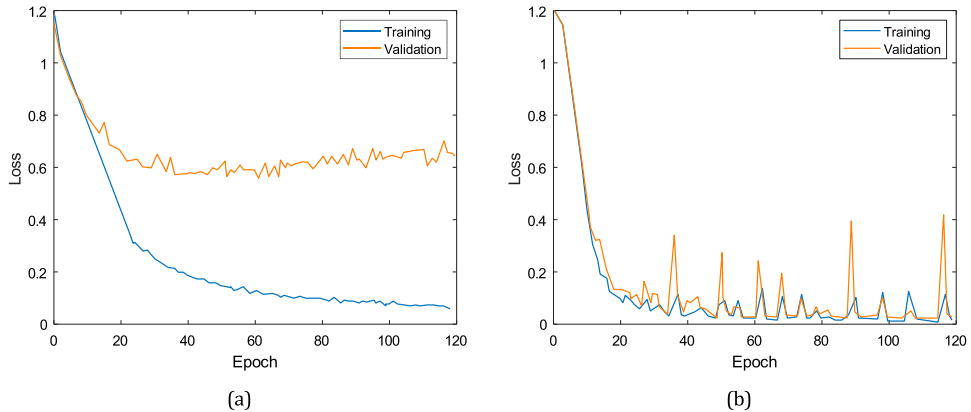


Figure 16. Loss plot of VMD-RP-DCNN (a) F1 (b) F2.

96.63%, which is comparatively larger than the specificity of the VDCNN. From the boxplot, we can note that the (RP) image input method with enhanced frame size offers better performance than the time series based input method with VDCNN. The key reason for the improved performance of VMD-RP-DCNN with *F2* is that large frame size contains more discriminative biomarkers for input classification. Moreover, unlike VDCNN which processes each VGRF sensor data individually, the VMD-RP-DCNN, which receives the RP of the dominant IMFs, can extract both spatial and temporal information. Hence, the DCNN with RP learns more discriminative features and offers significant improvement in PD severity classification. Finally, Table 5 gives the comparative analysis of the proposed framework with those of the previous approaches that have used gait pattern for PD diagnosis. We can note that the proposed approach outperforms the other approaches and is effective in classifying the three stages of PD. For instance, Ertuğrul et al. (2016) utilised the similar dataset used in our study and employed multilayer perceptron (MLP) to implement only binary classification. However, in this study, we have demonstrated that the proposed scheme can perform multi-class classification and predict the severity rating of PD based on H&Y scale by extracting the dominant spatio-temporal features of gait from RP. Furthermore, it can be noted

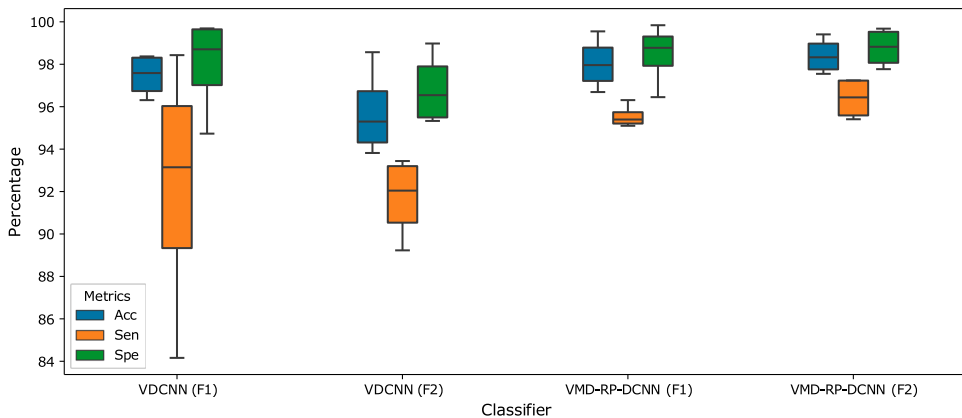


Figure 17. Key performance metrics of VCNN and RP-DCNN for different frame sizes.

Table 5. Performance comparison of proposed framework with other similar methods based on gait classification.

References	Features	Classifiers	Acc (%)	Sen (%)	Spe (%)
Ertuğrul et al. (2016)	Local binary patterns	MLP	88.8	88.9	82.2
Perumal and Sankar (2016)	Spatiotemporal	LDA	87.5	72.0	81.0
Wu et al. (2017)	Entropy parameters	SVM	84.48	72.41	96.5
Zeng et al. (2016)	Deterministic learning	RBF NN	96.39	96.77	95.89
Khoury et al. (2019)	Spatiotemporal	RF	90.91	85.35	88.35
El Maachi et al. (2020)	Spatial	CNN	85.22	85.28	87.29
Veeraragavan et al. (2020)	Spatiotemporal	ANN	87.11	90.48	67.89
Balaji et al. (2021)	Temporal	LSTM	96.61	96.19	98.10
Proposed	RP features	DCNN	98.45	96.38	98.77

that unlike the machine learning based approaches, reported in Ref. Khoury et al. (2019), Wu et al. (2017) and Perumal and Sankar (2016), which need the manual feature selection, the proposed DCNN avoids the necessity for manual features and extracts the important biomarkers automatically from the gait pattern.

5.2. Limitation of the proposed approach

The proposed VMD-RP-DCNN architecture for PD severity classification can be applied for assessing the only motor impairments of subjects who can walk. Hence, for predicting the severity of subjects above stage 4, the non-motor assessments based on UPDRS can be performed. Moreover, this study has majorly focused only on gait impairment for PD severity prediction. However, the multi-modal physiological signals such as tremor, speech and handwriting can be augmented to enhance the effectiveness of the DL classifier models.

6. Conclusions

This paper has described how non-invasive foot worn sensors can be combined with the deep learning technique to diagnose and predict the severity of PD through gait signal classification. Clinicians majorly diagnose PD through physical examination and clinical

assessment of symptoms. Nevertheless, misdiagnoses are inexorable because the assessment of PD is largely dependent on the expertise of the neurologists. Hence, to design a decision support system which can help the neurologists for PD diagnosis, we have presented a VGRF sensor-based gait abnormality analysis using VMD-RP-DCNN architecture that fuses the feature extraction and classification into a unified framework. Through VMD and spectral analysis, the VGRF signals have been decomposed and the IMFs that contain the prominent gait biomarkers have been extracted to form recurrence images. Subsequently, the RP of dominant IMFs have been used to train the DCNN to predict the severity of PD based on H&Y scale. To optimise the loss function, an Adam optimiser has been employed and the performance of the DCNN classifier model has been tested on Keras platform for two different input frames. Comparative analysis of the performance of proposed VMD-RP-DCNN with those of the other state-of-the-art techniques corroborate that our approach not only improves the classifier accuracy but also reduces the computational complexity by utilising the prominent IMFs for training DCNN. As a further study in this direction, to evaluate the motor impairments in PD subjects, the multi-modal assessment, which can utilise the gait, speech and tremor dataset, will be performed and the non-motor symptoms through the UPDRS score will be evaluated.

Disclosure statement

No potential conflict of interest was reported by the author(s).

References

- Abdulhay, E., Arunkumar, N., Narasimhan, K., Vellaiappan, E., & Venkatraman, V. (2018). Gait and tremor investigation using machine learning techniques for the diagnosis of Parkinson disease. *Future Generation Computer Systems*, 83, 366–373. <https://doi.org/10.1016/j.future.2018.02.009>
- Acharya, U. R., Oh, S. L., Hagiwara, Y., Tan, J. H., Adeli, H., & Subha, D. P. (2018). Automated eeg-based screening of depression using deep convolutional neural network. *Computer Methods and Programs in Biomedicine*, 161, 103–113. <https://doi.org/10.1016/j.cmpb.2018.04.012>
- Alharthi, A. S., & Ozanyan, K. B. (2019). Deep learning for ground reaction force data analysis: Application to wide-area floor sensing. In *2019 IEEE 28th International Symposium on Industrial Electronics (ISIE)* (pp. 1401–1406). IEEE.
- Alharthi, A. S., Yunas, S. U., & Ozanyan, K. B. (2019). Deep learning for monitoring of human gait: A review. *IEEE Sensors Journal*, 19, 9575–9591. <https://doi.org/10.1109/JSEN.7361>
- Arcos-García, Á., Alvarez-Garcia, J. A., & Soria-Morillo, L. M. (2018). Deep neural network for traffic sign recognition systems: An analysis of spatial transformers and stochastic optimisation methods. *Neural Networks*, 99, 158–165. <https://doi.org/10.1016/j.neunet.2018.01.005>
- Arifoglu, D., & Bouchachia, A. (2019). Detection of abnormal behaviour for dementia sufferers using convolutional neural networks. *Artificial Intelligence in Medicine*, 94, 88–95. <https://doi.org/10.1016/j.artmed.2019.01.005>
- Balaji, E., Brindha, D., & Balakrishnan, R. (2020). Supervised machine learning based gait classification system for early detection and stage classification of Parkinson's disease. *Applied Soft Computing*, 94, Article 106494. <https://doi.org/10.1016/j.asoc.2020.106494>
- Balaji, E., Brindha, D., Elumalai, V. K., & Vikrama, R. (2021). Automatic and non-invasive Parkinson's disease diagnosis and severity rating using LSTM network. *Applied Soft Computing*, 108, Article 107463. <https://doi.org/10.1016/j.asoc.2021.107463>
- Basha, S. S., Dubey, S. R., Pulabaigari, V., & Mukherjee, S. (2020). Impact of fully connected layers on performance of convolutional neural networks for image classification. *Neurocomputing*, 378, 112–119. <https://doi.org/10.1016/j.neucom.2019.10.008>

- Beigi, O. M., Nóbrega, L. R., Houghten, S., Pereira, A. A., & A. de Oliveira Andrade (2023). Freezing of gait in Parkinson's disease: Classification using computational intelligence. *Bio Systems*, 232, Article 105006. <https://doi.org/10.1016/j.biosystems.2023.105006>
- Camps, J., Sama, A., Martin, M., Rodriguez-Martin, D., Perez-Lopez, C., Arostegui, J. M. M., Cabestany, J., Catala, A., Alcaine, S., Mestre, B., Prats, A., Crespo-Maraver, M. C., Counihan, T. J., Browne, P., Quinlan, L. R., Laighin, G.Ó., Sweeney, D., Lewy, H., Vainstein, G., & Costa, A. (2018). Deep learning for freezing of gait detection in Parkinson's disease patients in their homes using a waist-worn inertial measurement unit. *Knowledge-Based Systems*, 139, 119–131. <https://doi.org/10.1016/j.knosys.2017.10.017>
- Eckmann, J. P., Kamphorst, S. O., & Ruelle, D. (1995). Recurrence plots of dynamical systems. *World Scientific Series on Nonlinear Science Series A*, 16, 441–446. <https://doi.org/10.1142/WSSNSA>
- El Maachi, I., Bilodeau, G. A., & Bouachir, W. (2020). Deep 1d-convnet for accurate Parkinson disease detection and severity prediction from gait. *Expert Systems with Applications*, 143, Article 113075. <https://doi.org/10.1016/j.eswa.2019.113075>
- Ertuğrul, Ö. F., Kaya, Y., Tekin, R., & Almalı, M. N. (2016). Detection of Parkinson's disease by shifted one dimensional local binary patterns from gait. *Expert Systems with Applications*, 56, 156–163. <https://doi.org/10.1016/j.eswa.2016.03.018>
- Fawaz, H. I., Forestier, G., Weber, J., Idoumghar, L., & Muller, P. A. (2019). Deep learning for time series classification: A review. *Data Mining and Knowledge Discovery*, 33, 917–963. <https://doi.org/10.1007/s10618-019-00619-1>
- Figueiredo, J., Santos, C. P., & Moreno, J. C. (2018). Automatic recognition of gait patterns in human motor disorders using machine learning: A review. *Medical Engineering & Physics*, 53, 1–12. <https://doi.org/10.1016/j.medengphy.2017.12.006>
- Frenkel-Toledo, S., Giladi, N., Peretz, C., Herman, T., Gruendlinger, L., & Hausdorff, J. M. (2005). Treadmill walking as an external pacemaker to improve gait rhythm and stability in Parkinson's disease. *Movement Disorders: Official Journal of the Movement Disorder Society*, 20, 1109–1114. <https://doi.org/10.1002/mds.v20:9>
- Hausdorff, J. M., Lowenthal, J., Herman, T., Gruendlinger, L., Peretz, C., & Giladi, N. (2007). Rhythmic auditory stimulation modulates gait variability in Parkinson's disease. *European Journal of Neuroscience*, 26, 2369–2375. <https://doi.org/10.1111/ejn.2007.26.issue-8>
- He, T., Liu, Y., Yu, Y., Zhao, Q., & Hu, Z. (2020). Application of deep convolutional neural network on feature extraction and detection of wood defects. *Measurement*, 152, Article 107357. <https://doi.org/10.1016/j.measurement.2019.107357>
- Hou, S., Xu, Y., & Guo, W. (2022). Distribution network fault-line selection method based on miceem-dan-recurrence plot-yolov5. *Processes*, 10, 2127. <https://doi.org/10.3390/pr10102127>
- Joshi, D., Khajuria, A., & Joshi, P. (2017). An automatic non-invasive method for Parkinson's disease classification. *Computer Methods and Programs in Biomedicine*, 145, 135–145. <https://doi.org/10.1016/j.cmpb.2017.04.007>
- Khera, P., & Kumar, N. (2022). Age-gender specific prediction model for Parkinson's severity assessment using gait biomarkers. *Engineering Science and Technology, an International Journal*, 27, Article 101005. <https://doi.org/10.1016/j.jestch.2021.05.009>
- Khouri, N., Attal, F., Amirat, Y., Oukhellou, L., & Mohammed, S. (2019). Data-driven based approach to aid Parkinson's disease diagnosis. *Sensors*, 19, 1–27. <https://doi.org/10.3390/s19020242>
- Kim, H. B., Lee, W. W., Kim, A., Lee, H. J., Park, H. Y., Jeon, H. S., Kim, S. K., Jeon, B., & Park, K. S. (2018). Wrist sensor-based tremor severity quantification in Parkinson's disease using convolutional neural network. *Computers in Biology and Medicine*, 95, 140–146. <https://doi.org/10.1016/j.combiomed.2018.02.007>
- Oung, Q. W., Muthusamy, H., Basah, S. N., Lee, H., & Vijean, V. (2018). Empirical wavelet transform based features for classification of Parkinson's disease severity. *Journal of Medical Systems*, 42, 1–17. <https://doi.org/10.1007/s10916-017-0877-2>
- PD: P.D.D. (2020). Available online: <https://www.physionet.org/content/gaitpdb/1.0.0/>.
- Pereira, C. R., Pereira, D. R., Rosa, G. H., Albuquerque, V. H., Weber, S. A., Hook, C., & Papa, J. P. (2018). Handwritten dynamics assessment through convolutional neural networks: An

- application to Parkinson's disease identification. *Artificial Intelligence in Medicine*, 87, 67–77. <https://doi.org/10.1016/j.artmed.2018.04.001>
- Perumal, S. V., & Sankar, R. (2016). Gait and tremor assessment for patients with Parkinson's disease using wearable sensors. *Ict Express*, 2, 168–174. <https://doi.org/10.1016/j.icte.2016.10.005>
- Prabhu, P., Karunakar, A. K., Anitha, H., & Pradhan, N. (2020). Classification of gait signals into different neurodegenerative diseases using statistical analysis and recurrence quantification analysis. *Pattern Recognition Letters*, 139, 10–16.
- Saba, L., Biswas, M., Kuppili, V., Godia, E. C., Suri, H. S., Edla, D. R., Omerzu, T., Laird, J. R., Khanna, N. N., Mavrogeni, S., Protoplerou, A., Sfikakis, P. P., Viswanathan, V., Kitas, G. D., Nicolaides, A., Gupta, A., & Suri, J. S. (2019). The present and future of deep learning in radiology. *European Journal of Radiology*, 114, 14–24. <https://doi.org/10.1016/j.ejrad.2019.02.038>
- San-Segundo, R., Gil-Martín, M., D'Haro-Enríquez, L. F., & Pardo, J. M. (2019). Classification of epileptic eeg recordings using signal transforms and convolutional neural networks. *Computers in Biology and Medicine*, 109, 148–158. <https://doi.org/10.1016/j.combiomed.2019.04.031>
- Schwab, P., & Karlen, W. (2019). *PhoneMD: Learning to diagnose Parkinson's disease from smartphone data*. Proceedings of the AAAI conference on artificial intelligence (Vol. 33, No. 01, pp. 1118–1125).
- Shankar, A., Khaing, H. K., Dandapat, S., & Barma, S. (2021). Analysis of epileptic seizures based on eeg using recurrence plot images and deep learning. *Biomedical Signal Processing and Control*, 69, Article 102854. <https://doi.org/10.1016/j.bspc.2021.102854>
- Shuzan, M. N. I., Chowdhury, M. E., Reaz, M. B. I., Khandakar, A., Abir, F. F., M. A. A. Faisal, Ali, S. H. M., Bakar, A. A. A., Chowdhury, M. H., Mahbub, Z. B., Uddin, M. M., & Alhatou, M. (2023). Machine learning-based classification of healthy and impaired gaits using 3d-grf signals. *Biomedical Signal Processing and Control*, 81, Article 104448. <https://doi.org/10.1016/j.bspc.2022.104448>
- Skaramagkas, V., Pentari, A., Kefalopoulou, Z., & Tsiknakis, M. (2023). Multi-modal deep learning diagnosis of Parkinson's disease-a systematic review. *IEEE Transactions on Neural Systems and Rehabilitation Engineering*, 31, 2399–2423.
- ul Haq, A., J. P. Li, Agbley, B. L. Y., Mawuli, C. B., Ali, Z., Nazir, S., & Din, S. U. (2022). A survey of deep learning techniques based Parkinson's disease recognition methods employing clinical data. *Expert Systems with Applications*, 208, Article 118045. <https://doi.org/10.1016/j.eswa.2022.118045>
- Vásquez-Correa, J. C., Arias-Vergara, T., Orozco-Arroyave, J., Eskofier, B., Klucken, J., & Nöth, E. (2018). Multimodal assessment of Parkinson's disease: A deep learning approach. *IEEE Journal of Biomedical and Health Informatics*, 23, 1618–1630. <https://doi.org/10.1109/JBHI.6221020>
- Veeraragavan, S., Gopalai, A. A., Gouwanda, D., & Ahmad, S. A. (2020). Parkinson's disease diagnosis and severity assessment using ground reaction forces and neural networks. *Frontiers in Physiology*, 11, 1–11. <https://doi.org/10.3389/fphys.2020.587057>
- Vidya, B., & Sasikumar, P. (2021). Gait based Parkinson's disease diagnosis and severity rating using multi-class support vector machine. *Applied Soft Computing*, 113, Article 107939. <https://doi.org/10.1016/j.asoc.2021.107939>
- Wu, Y., Chen, P., Luo, X., Wu, M., Liao, L., Yang, S., & Rangayyan, R. M. (2017). Measuring signal fluctuations in gait rhythm time series of patients with Parkinson's disease using entropy parameters. *Biomedical Signal Processing and Control*, 31, 265–271. <https://doi.org/10.1016/j.bspc.2016.08.022>
- Xia, Y., Zhang, J., Ye, Q., Cheng, N., Lu, Y., & Zhang, D. (2018). Evaluation of deep convolutional neural networks for detection of freezing of gait in Parkinson's disease patients. *Biomedical Signal Processing and Control*, 46, 221–230. <https://doi.org/10.1016/j.bspc.2018.07.015>
- Yogev, G., Giladi, N., Peretz, C., Springer, S., Simon, E. S., & Hausdorff, J. M. (2005). Dual tasking, gait rhythmicity, and Parkinson's disease: Which aspects of gait are attention demanding? *European Journal of Neuroscience*, 22, 1248–1256. <https://doi.org/10.1111/ejn.2005.22.issue-5>
- Zeng, W., Liu, F., Wang, Q., Wang, Y., Ma, L., & Zhang, Y. (2016). Parkinson's disease classification using gait analysis via deterministic learning. *Neuroscience Letters*, 633, 268–278. <https://doi.org/10.1016/j.neulet.2016.09.043>
- Zhou, T., Ruan, S., & Canu, S. (2019). A review: Deep learning for medical image segmentation using multi-modality fusion. *Array*, 3, Article 100004. <https://doi.org/10.1016/j.array.2019.100004>